A PSO-ABC ALGORITHM OF PID PARAMETER TUNING FOR LEVITATION CONTROL OF DIVING ROBOTS

Yu Huang, Shan Xue, Xiang Yao, Hongyan Chen*
School of Information and Communication Engineering, Hainan University, Haikou 570228, China

Abstract - A combined particle swarm optimization and artificial bee colony algorithm (PSO-ABC) is designed. Compared with the traditional particle swarm optimization (PSO), artificial bee colony algorithm (ABC), genetic algorithm (GA) and frog leaping algorithm (FLA), this algorithm has a significant advantage in the average (AVG) and standard deviation (STD) of the convergence degree of multiple experiments and the process of PID controller parameter tuning. Then the diving robot model with ballast tank as the core is constructed, and the algorithm is used for the PID controller parameter tuning of the robot levitation link, which is used to correct the error of the robot diving process, so as to ensure that the robot stably maintains at a specific water depth. The reliability of the PID controller designed by this algorithm is finally verified by computer simulation.

Keywords: PSO-ABC; diving robot; Ballast tank; Levitation control; PID controller parameter tuning.

1. Introduction

Diving robots play an important role in industrial production, scientific research work, and other aspects [1]. At present, the common robot or equipment diving is mainly realized by the following two ways. The first is to use only the propeller to dive, this type of equipment diving process requires the propeller force and equipment gravity to overcome its own buoyancy, so it is more energy-consuming. Common diving drones work in this way. The second type is by carrying ballast tanks, the vertical direction of the diving process can rely on the water intake and drainage process to realize. This type of submersible also requires a propeller to be fitted to assist in achieving movement in the horizontal plane. For example, submarines use this type of program. This paper focuses on the underwater levitation control in the vertical plane, which is also its technical difficulty and core problem. The response speed, accuracy and stability of the robot's underwater levitation at a specific location need to be repeatedly debugged, and it is not a permanent solution to directly determine the position of the diving robot underwater by means of observation.

With the progress of computer science, bio-heuristic algorithms have flourished [2]. Particle swarm optimization (PSO) finally solves complex optimization problems by simulating the foraging behavior of bird flocks in nature. Artificial bee colony algorithm (ABC), originating from the behavior of honey bees in collecting honey, has good global and local search capability. Additionally, other types of bio-heuristic algorithms play a pivotal role in solving optimization problems. Genetic algorithm (GA) achieves the search for optimal solutions by simulating the laws of genetics in nature. Frog leaping algorithm (FLA) gives a solution to combinatorial optimization problems by simulating the foraging behavior of frog population.

PID control is the correction of proportional, integral, and differential for system-generated errors [3]. Its structure is simple, robust, widely used in various types of industrial production. However, the parameter tuning process of PID controller is a difficult problem. In addition to the traditional manual parameter tuning method, it also includes Ziegler-Nichols method [4], frequency domain analysis method [5], combined with intelligent optimization algorithm calibration, etc. Ziegler-Nichols method is a classical PID parameter calibration method, which is simple and easy to operate, but its implementation process relies on the actual experimental test, which is an empirical method. The frequency domain analysis method requires the frequency response test of the system. And plot the Nyquist, then analyze and adjust the PID controller parameters. This method also belongs to the classical control field, and is not suitable for computer-aided mass computation.

Therefore, in this paper, a bio-heuristic algorithm (a class of intelligent optimization algorithms) is used

https://doi.org/10.17683/ijomam/issue22.v1.25

to parameterize the PID controller of the levitation process of a diving robot, which not only saves the manpower cost of manually adjusting the parameters and improves the efficiency of the robot, but also is suitable for computer simulation and large-scale computation. This paper uses the PSO-ABC algorithm. Differing from the traditional algorithms, the algorithm in the degree of convergence of multiple experiments, the standard deviation (STD), and PID controller parameter tuning has a significant advantage.

In addition to the application in the case of levitation control of diving robots, in order to tune the PID controller parameters of the control system, researchers have proposed a variety of intelligent algorithms for optimization. The following are examples of bio-heuristic algorithms: Ahmadnia et al [6] designed a novel fractional order PID controller tuned using a hybrid PSO that outperforms current fractional and integer order PID controllers in terms of performance and transient response. Saravanakumar et al [7] designed a new PID controller for managing and controlling the postoperative care in the T1D insulin injections with an IMO-PSO FO-PID controller, which efficaciously improves glycemic control. Baz et al [8] provide an avenue, by synergizing PSO with PID and fuzzy control to enhance the speed control system of a brushless DC motor-powered electric vehicle. Masikana [9] provides a new approach to the speed control system of a brushless DC motor-powered electric vehicle by considering the IAE, ITAE, and ITSE mis-defined stochastic fractional search algorithm to optimize the gain of PID, the robustness of the method was also validated for different magnitudes of random load variations and a wider range of parameter variations. Amudipe et al [10] investigated the use of slime mold algorithms for tuning the PID controller settings of a dynamic system, the efficiency of the slime mold algorithm in optimizing the parameters of the PID controller improved the control robustness and performance. Ghith et al [11] applied a novel hybrid algorithm based on arithmetic optimization algorithm and artificial gorilla force optimization to a micro-robotic system and obtained the best PID controller parameters.

Additionally, researchers have also used other optimization strategies. Liu et al [12] proposed a model-free adaptive control method PID algorithm for pH neutralization process, and the proposed MFAC-SA-PID method has a better control effect on the pH neutralization process. Long et al [13] proposed a PID controller tuned with a dung beetle optimizer, which was applied to quickly and stably control the surface back pressure. Cheng [14] et al optimized a tracking system for heading deviation angle and designed a model-free adaptive predictive control proportional-integral derivative method, improving the operating accuracy of tractor autopilot. Çelik [15] introduced an exponential PID controller as a new control scheme to improve the power system's performance of load frequency regulation. Wang [16] used a fuzzy strategy to optimize the PID control of an electronic expansion valve on a single-pipe heat exchanger experimental platform. Compared with the conventional PID control, the fuzzy PID control has reduced overshoot, shorter regulation time and smaller range of superheat fluctuation. Wang [17] proposed a soft actor-critic based adaptive PID controller for AUV path tracking. This controller combines the interpretability of PID with the intelligence of reinforcement learning. Leninpugalhanthi et al [18] proposed a direct torque control based on an adaptive PID controller. The proposed controller relies on the extra error indicated by the rotary controller to comprehend the nonlinearities, parameter fluctuations, and burden transfer difficulties that occur in the brushless DC motor drive framework to keep up good torque control performance. Wang et al [19] utilized the contraction property of the port-Hamiltonian system to propose a trajectory tracking PID passivity-based control method, which effectively solves the trajectory tracking problem of the ground dynamics around the L2 point in the port-Hamiltonian framework. Hu et al [20] proposed a new internal model PID controller design method for the load-frequency control system of the power grid centered on pole-zero transition, which aims to simplify the complexity of the system model and improve the performance of the system. Chen et al [21] combined a vertical motion prediction algorithm based on an autoregressive integrated moving average (AVG) model with a nonlinear model predictive control method. The cascade structure is introduced due to its rapid error response to control lags and effective system downscaling to reduce the computational burden, which lays an important foundation for real-time regulation of PID gains based on a nonlinear model predictive control method that ensures the secondary regulated active heave compensation system evolves optimally while improving its practical feasibility. Coskun [22] et al designed an intelligent PID controller for implementing position control of nonlinear electrohydraulic systems with uncertain valve characteristics and varying supply pressure.

The work of this paper includes the following aspects:

(1) This paper systems modeling of levitation control of diving robots, and proposes a feasible scheme - a levitation method of a diving robot based on ballast tank control, by adjusting the water level in the tank to ensure levitation at a specific depth underwater.

(2) This paper proposes a PSO-ABC algorithm, which bio-heuristic algorithm is used to parameterize the PID controller for the levitation process of the submersible robot.

(3) Compare the performance of PSO-ABC algorithm with the traditional bio-heuristic algorithm. By traditional PSO, ABC, GA as well as FLA and comparing AVG, STD of their multiple experiments and the process of parameter tuning of the PID controller, the significant effect of the algorithm is verified. Finally, a simulation model is constructed to verify the reliability of the PID controller obtained by the algorithm.

2. Prerequisite Knowledge

2.1 Traditional PSO and ABC Algorithm

In PSO [23], the initial position of any particle is randomly generated. The position X_i of any particle in 3D space is as follows $(i = 1, 2, \ldots\ldots, N)$:

$$X_i = (x_{i1}, x_{i2}, x_{i3}) \tag{1}$$

The speed V_i of each of them is as follows:

$$V_i = (v_{i1}, v_{i2}, v_{i3}) \tag{2}$$

The optimal position it has searched so far is the individual extremum p_{best}, and the formula is as follows:

$$p_{best} = (p_{i1}, p_{i2}, p_{i3}) \tag{3}$$

The optimal position searched so far by the whole swarm of particles is the global extremum g_{best} with the following equation:

$$g_{best} = (g_{i1}, g_{i2}, g_{i3}) \tag{4}$$

An arbitrary particle updates the velocity v_{ij} and position x_{ij} by comparing the individual poles with the global poles:

$$v_{ij}(t+1) = w \cdot v_{ij}(t) + c_1 r_1(t) \cdot [p_{ij}(t) - x_{ij}(t)] + c_2 r_2(t) \cdot [p_{gj}(t) - x_{ij}(t)] \tag{5}$$

$$x_{ij}(t+1) = x_{ij}(t) + v_{ij}(t+1) \tag{6}$$

where w is the inertia weight; c_1, c_2 are the learning factors; r_1, r_2 are uniform random numbers in $[0,1]$; v_{ij} is the velocity of the particle, which ranges from $[-v_{max}, v_{max}]$; and j denotes the dimensionality $(j = 1, 2, 3)$.

According to (5) and (6), any particle completes each search, and the particle swarm can obtain the optimal solution within a sufficiently large number of iterations.

In the ABC [24], the initial nectar source location x_{id} is randomly generated as follows:

$$x_{id} = L_d + r_1(t) \cdot (U_d - L_d) \tag{7}$$

where L_d and U_d denote the upper and lower boundaries of traversal respectively.

The colony structure in the ABC consists of three types: leading bees, following bees, and scout bees. The leading bee searches for nectar around nectar source i in the following way x_{id}^{new} $(j \neq i)$:

$$x_{id}^{new} = x_{id} + a \cdot r(t) \cdot (x_{id} - x_{jd}) \tag{8}$$

where $r(t)$ is a uniform random number in [0,1] and a is the acceleration factor (usually taken as 1). The following bees choose the leading bees and also conform to the roulette rule with the same probability formula as in (9).

After n iterations of search, if the nectar source reaches the threshold L but has not been updated to a better source, the scout bees will then abandon the nectar source and instead find a new nectar source with the location x_i of the new nectar source:

$$x_i = L_d + r(t) \cdot (U_d - L_d) \tag{9}$$

The number of iterative searches is less than a threshold L, the honey source keeps its position unchanged. Within a sufficiently large number of iterations, the bee colony can achieve the optimal solution of the objective function.

2.2 PID Controller

PID is an algorithm for control by means of proportional, differential and integral calculations, and its control principle is shown in Figure 1. The standard PID control value is proportional to the deviation (the difference between the set value of the control system and the actual value), the integral of the deviation to the time, and the differential of the deviation to the time, and the sum of the three. The formula is as follows:

$$U(t) = K_p e(t) + K_i \int e(t)dt + K_d \frac{de(t)}{dt} \tag{10}$$

where K_p is the proportionality coefficient; K_i is the integration coefficient; K_d is the differentiation coefficient.

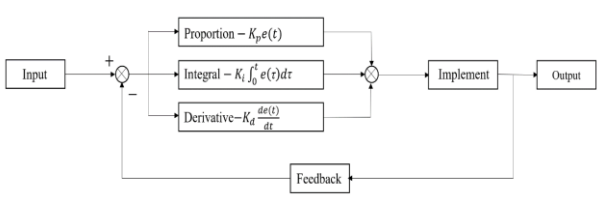

Figure 1: Closed-loop control schematic diagram

Proportional adjustment is to quickly adjust to the desired value by multiplying the proportional value. Integral regulation is the process of converging the target to the desired value by setting an integral

amount and continuously integrating the deviation according to the presence of the deviation.

Differential regulation smoothens the process of adjustment by providing a damping.

$e(t)$ is the inaccuracy. It is a function of time t. The defining equation is as follows:

$$e(t) = r(t) - y(t) \tag{11}$$

where $r(t)$ is the expected value; $y(t)$ is the actual value.

The Laplace transform of the PID controller is expressed as follows:

$$G_c(s) = \frac{U(s)}{E(s)} = K_P + K_i \frac{1}{s} + K_d s \tag{12}$$

2.3 Error Integration Criterion

The basic error integral type fitness functions include the integral of the square of the error (ISE), the integral of the square of the time multiplied by the error (ITSE), the integral of the absolute value of the error (IATE) and the integral of the absolute value of the time multiplied by the error (ITAE). The definition is as follows:

$$ISE = \int_0^\infty e^2(t)dt \tag{13}$$

$$ITSE = \int_0^\infty te^2(t)dt \tag{14}$$

$$IAE = \int_0^\infty |e(t)|dt \tag{15}$$

$$ITAE = \int_0^\infty t|e(t)|dt \tag{16}$$

ISE is the most commonly used fitness function, which requires high stability of the system. ITSE takes into account the speed and stability of convergence. IAE has suppression effect on the overshooting amount. ITAE not only further represses the overshooting amount, but also has the shortest rise time. For the first-order inertial system, the system unit step response overshoot is small, and it has good stability itself, and the calculation is simple. Therefore, this article adopts the ISE as the fitness function.

3. Results

3.1 Transfer Function Construction

According to Archimedes' principle, the buoyant force on an object is equal to the gravitational force of the liquid it displaces. Underwater position-specific levitation of diving robots requires the use of ballast tanks with water intake and dewatering functions, thus changing the force state of the diving robot. There is a mapping relationship between the water level in the ballast tank and the suspension of the submersible robot at a specific location underwater, and the mapping relationship can be found by making a physical model to measure the corresponding values. Here in this paper, the water level height in the ballast tank is directly used to characterize the robot levitation height.

The schematic diagram of the ballast tank is shown in Figure 2, which is the most central component of the diving robot to realize the levitation function. Its relative position in the robot is shown in Figure 3, where the influence of other parts on the robot's levitation function is ignored, where A is the bottom area of the ballast tank; q_i and q_o are the water intake and discharge, respectively, which are functions of time t; V is the water storage capacity of the ballast tank; h_o is the steady state height of the water level. According to the material dynamic equilibrium relationship, there is the following equation:

$$q_i - q_o = \frac{dV}{dt} = A\frac{dh}{dt} \tag{17}$$

According to the equations of kinematics, the relationship between the discharge q_o and the steady-state height of the water level h is nonlinear, and can be linearized near the equilibrium point (h_o, q_o), resulting in an expression for the discharge:

$$q_o \approx C \cdot \sqrt{h_o} + \frac{C \cdot (h - h_o)}{2\sqrt{h_o}} \tag{18}$$

By substituting Eq. (18) into Eq. (17), it can be approximated as a first order linear system:

$$q_i - \frac{C}{2\sqrt{h_o}} h = A\frac{dh}{dt} \tag{19}$$

The Laplace transform of Eq. (19) results in the following transfer function equation:

$$G(s) = \frac{1}{As + \frac{C}{2\sqrt{h_o}}} \tag{20}$$

Show that the model is an inertial system with the following expression:

$$G(s) = \frac{K}{Ts + 1} \tag{21}$$

where the time constant is $T = \frac{2A}{C}\sqrt{h_o}$, the open-loop gain is $K = \frac{2}{C}\sqrt{h_o}$.

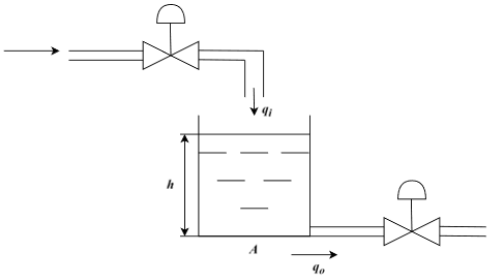

Figure 2: Schematic diagram of ballast tanks

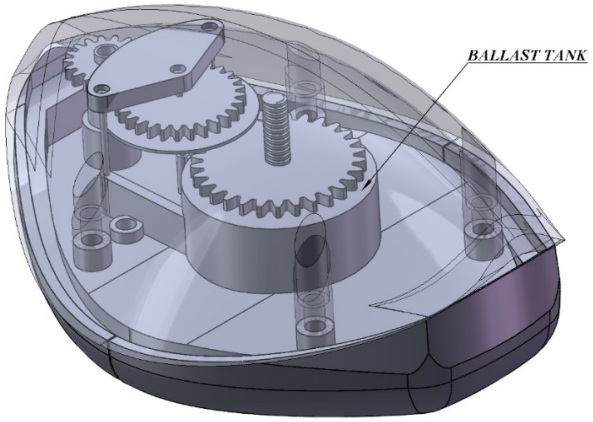

Figure 3: Position of ballast tanks relative to the diving robot.

For the diving robots explored in this paper, the parameters related to their ballast tanks are specified as shown in Table 1:

Table 1. Parameters of Ballast Tanks for Diving Robots

Relevant physical quantity	Values
Ballast tank bottom area A	0.1
Outlet flow coefficient C	0.02
Set water level steady state height h_o	0.1

Substituting the parameters into Eq. (20) results in the expression for the transfer function under this model:

$$G(s)=\frac{1}{0.1s+\frac{0.02}{2\sqrt{0.1}}}\approx\frac{100}{3}\cdot\frac{1}{\frac{10}{3}s+1}$$

3.2 PSO-ABC Algorithm

The flowchart of a PSO-ABC Algorithm is shown in Figure 4. During each iteration of this algorithm, the PSO is first used globally to search for the global optimum and save the global optimum and its location at this time. Then the ABC is used to continue searching for the local optimal value in the neighborhood of the global optimal value found by the PSO. If the optimal value obtained by the ABC is due to the previously saved global optimal value, the global optimal value will be updated. On the contrary, the global optimum obtained by the PSO is still maintained. At this point, this iteration process ends and proceeds to the next iteration process. After completing all the iterations, the global optimal value is output, and finally the optimal value of the objective function is found corresponding to the PID tuning parameters.

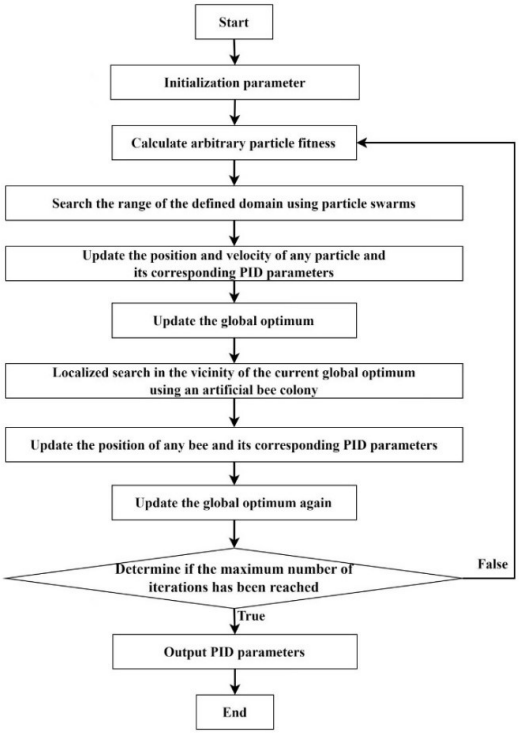

Figure 4: PSO-ABC flowchart

Because of this, for the diving robot underwater specific depth suspension process transfer function model, the algorithm in the early operation of the distribution of particles is more dispersed, and later gradually convergence process. Here the PSO needs to be regulated for each update of the particle velocity and position, depending on the inertia weights pre-designed by the PSO.

The inertia weights decrease with the iterative process, thus, weakening the step size of the particle search process, and converting from a global search to a fine search, which is in line with the ABC global optimum near the further search process. The inertia weight adjustment relation is as follows, where w is the inertia weight; m is the total number of iterations; n is the current number of iterations ($n=1,2,.....m$) :

$$w=0.9-0.8\frac{n}{m} \tag{22}$$

3.3 Adaptive Function

The optimal solution obtained by the bio-heuristic algorithm according to K_p, K_i and K_d is passed to the PID controller. By correcting the error of the process of ballast tank water inlet and outlet, the PID

controller realizes the suspension of diving robot at a specific position underwater. h_o is the steady state height of the water level; $h(t)$ is the height of the water level at a certain moment, and according to Eq. (11), the error is:

$$e(t) = h(t) - h_o$$

According to the error integration criterion, for inertial links in ballast tank modeling, which has a small oscillation of its own system response, the ISE can be used to characterize the performance evaluation index of the system. The fitness function of the water level at a certain moment $h(t)$ and water level steady height h_o difference, is taken as an infinite integral of the Euclidean paradigm with the following equation:

$$ISE = \int_0^{\infty} \|h(t) - h_o\|_2 \, dt \tag{23}$$

Index the bio-heuristic algorithm parameters and calculate its fitness function value each time the algorithm search is performed. The minimum value of the fitness function value and its relative PID parameter value are obtained, and the next iteration is performed in the direction of a smaller fitness function value. Finally, the PID parameter values converge at a specific position, at which time the PID controller can quickly, accurately and stably correct the ballast tank's inlet and outlet processes and realize the diving robot's suspension at a specific position underwater.

4. Simulation Verification

4.1 Benchmark Function Validation

In order to verify the effects of the proposed bio-heuristic algorithm in finding the optimal value, the algorithm is tested against the other four basic algorithms in the following, using the Sphere, Griewank, Zakharov, and SumSquares benchmark functions as the fitness functions. The AVG and STD of the fitness function after repeated experiments are obtained. The initialization parameters are shown in Table 2. Where, the "maximum number of iterations" indicates the upper limit of experimental cycles, while the "number of individuals in the algorithm" denotes the number of individuals involved in the iterative process of the five algorithms. The benchmark functions used are shown in Table 3:

The benchmark function test results are shown in Figure 5, Figure 6, and Table 4. Given that AVG represents the average of the optimal values of the function solved by the algorithm in each iteration, STD represents the degree of fluctuation in the values obtained from multiple iterations. For the four benchmark functions, it can be seen that after repeated experiments with the PSO-ABC algorithm, the AVG of the fitness function is closest to the true optimal value of 0. Taking the Sphere function as an example, the AVG value is 2.50E-14, which is one order of magnitude lower than the optimal results of the other four algorithms. The fluctuation of STD changes is the smallest. Taking the Sphere function as an example, the STD value is 4.37E-14, which is one order of magnitude lower than the optimal results of other algorithms. The above results reflect the characteristic of PSO-ABC in solving optimization problems, where multiple solutions yield more accurate and stable results.

Table 2. Initialization Parameters Table for Bio-heuristic Algorithm Benchmark Function Testing

Relevant parameters	Values
Maximum number of iterations	50
Number of individuals in the algorithm (PSO, ABC, GA, FLA, PSO-ABC)	100

Table 3. Table of Baseline Functions

Functions	Formulas	Domain	Optimum value
Sphere	$f(x) = \sum_{i=1}^{n} x_i^2$	$[-5.12, 5.12]$	0
Griewank	$f(x) = 1 + \frac{1}{4000}\sum_{i=1}^{n} x_i^2 - \prod_{i=1}^{n} \cos(\frac{x_i}{\sqrt{i}})$	$[-600, 600]$	0
Zakharov	$f(x) = \sum_{i=1}^{n} x_i^2 + \sum_{i=1}^{n} (0.5ix_i)^2 + \sum_{i=1}^{n} (0.5ix_i)^4$	$[-5, 10]$	0
SumSquares	$f(x) = \sum_{i=1}^{n} ix_i^2$	$[-10, 10]$	0

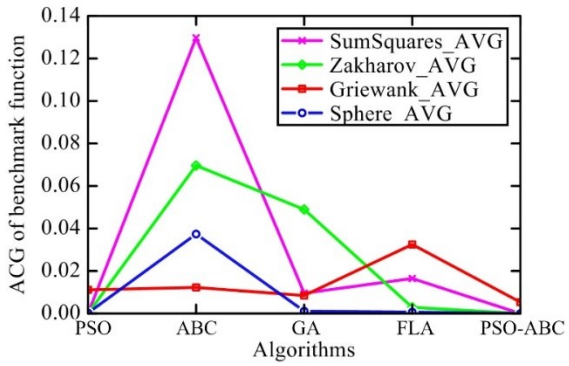

Figure 5. Bio-heuristic algorithm fitness function AVG control plot

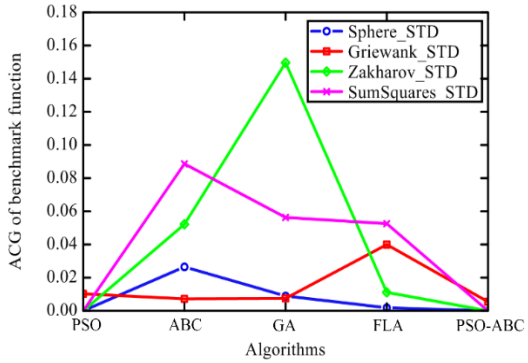

Figure 6. Bio-heuristic algorithm fitness function STD control plot

Table 4. Table 1Bio-heuristic Algorithm Benchmark Function Test Data Sheet

Algorithm	PSO		ABC		GA		FLA		PSO-ABC	
Function	AVG	STD	AVG	STD	AVG	STD	AVG	STD	AVG	STD
Sphere	1.58E-13	1.85E-13	0.037254	0.026299	1.11E-03	8.86E-03	0.00031537	0.0015013	**2.50E-14**	**4.37E-14**
Griewank	0.011032	0.01012	0.012169	0.0068758	0.0084615	0.0070514	0.032301	0.039577	**0.0054664**	**0.0049511**
Zakharov	3.13E-13	4.14E-13	0.069914	0.052174	4.91E-02	1.50E-01	0.0028291	0.011057	**4.46E-14**	**7.72E-14**
SumSquares	6.43E-13	9.24E-13	0.12992	0.088617	9.66E-03	5.59E-02	0.016584	0.052293	**1.24E-13**	**3.49E-13**

4.2 Simulation Verification of Levitation Process of Diving Robot

In order to verify the effect of the proposed bio-heuristic algorithm for the implementation of this transfer function PID controller parameter tuning process, the following is a comparison of the algorithm with the traditional PSO, ABC, GA, and FLA in the dive robot PID controller parameter tuning process parameters of the iterative convergence of the number of iterations, the value of the situation, and the simulation of the water level change in the ballast tanks, which is shown in the schematic of Figure 7. The initialization parameters of the five algorithms are set as shown in Table 5, and the results obtained are shown in Figure 8 to Figure 14:

Table 5. Initialisation Parameters for Convergence Effect of Four Intelligent Optimization Algorithms

Relevant parameters	Values
Maximum number of iterations	100
Number of individuals in the algorithm (PSO, ABC, GA, FLA, PSO-ABC)	1000

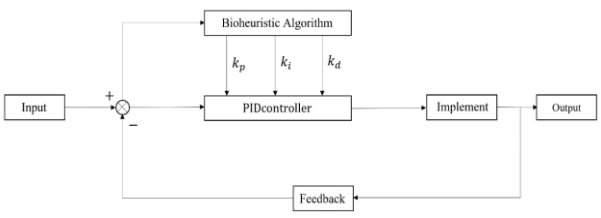

Figure 7: Schematic diagram of bio-heuristic algorithm for PID controller parameter correction

The effect of PID parameter tuning of PSO algorithm is shown in Figure 8, Figure 9 and Figure 14, and the final values of PID controller parameters converged are shown in Table 6. The algorithm's fitness function converges quickly, the PID controller parameters oscillate significantly at the beginning, and convergence is obtained after more than 10 iterations, eventually all the indicators are stabilized.

The effect of PID parameter tuning of ABC algorithm is shown in Figure 8, Figure 10 and Figure 14, and the final converged values of PID controller parameters are shown in Table 6. At this time, the fitness function, the PID controller parameters and the ballast tank water level all realize convergence. However, the PID controller parameters in the integral coefficient convergence speed is slightly slower, and its final results, the differential coefficient value role is limited, much smaller than the proportional coefficient, integral coefficient. Also, it is necessary to fully operate the three parameters, and the system is more complex.

The effect of PID parameter tuning of the GA algorithm is shown in Figure 8, Figure 11 and Figure 14, and the final PID controller parameters converge at the values is shown in Table 6. In this case, the oscillation of the PID parameters is obvious at the initial time of the algorithm, and when the number of iterations of the algorithm exceeds 20, the fitness function gets converged and the PID parameters likewise tend to converge. The ballast tank water level varies to a slightly greater extent. In the final PID controller parameters, the GA gives a set of values different from the PSO algorithm, at this time the controller needs to completely consider the 3 parameters, the design is relatively complex, for the whole system the design cost increases, and it is not the optimal solution.

The effect of PID parameter tuning of the FLA algorithm is shown in Figure 8, Figure 12 and Figure 14, and the final values of the PID controller parameters converged are shown in Table 6. At this time, the fitness function, PID controller parameters and ballast tank water level all realize convergence. However, the convergence of the PID controller parameters is significantly slower than that of the PSO algorithm. The degree of change of ballast tank water level is slightly larger.

The effect of PID parameter tuning of PSO-ABC algorithm is shown in Figure 8, Figure 13 and Figure 14, and the final converged values of PID controller parameters are shown in Table 6. At this time, the fitness function, PID controller parameters and ballast tank water level all realize convergence. the PID controller parameters change rapidly and directly during the convergence process, and the oscillation amplitude is small, which is obviously better than the traditional PSO algorithm and ABC algorithm and other traditional bio-heuristic algorithms. In summary, the use of PSO-ABC for PID controller for robot underwater depth-specific suspension control model is superior.

Table 6. Numerical convergence of PID controller parameters for five algorithms

PID controller parameters	PSO value	ABC value	GA value	FLA value	PSO-ABC value
Proportional	9.9368	9.9368	2.5718	9.9371	9.9368
Integral	6.3246	6.3246	6.3801	6.3231	6.3246
Derivative	0	6.8321e-10	0.073887	0	0

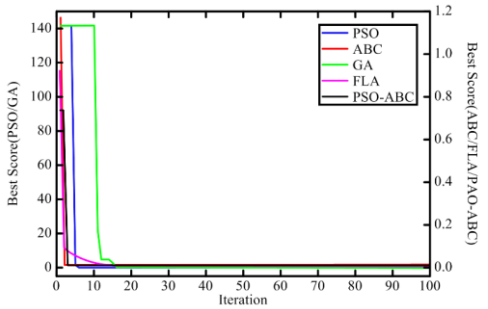

Figure 8: Convergence of five algorithms fitness function

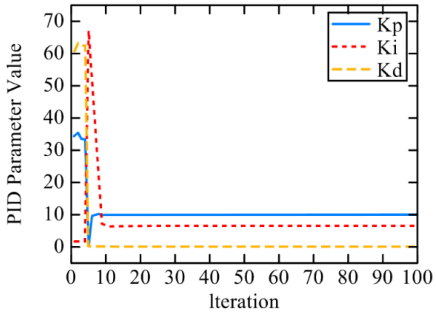

Figure 9: Convergence effect of parameter adjustment of PSO algorithm

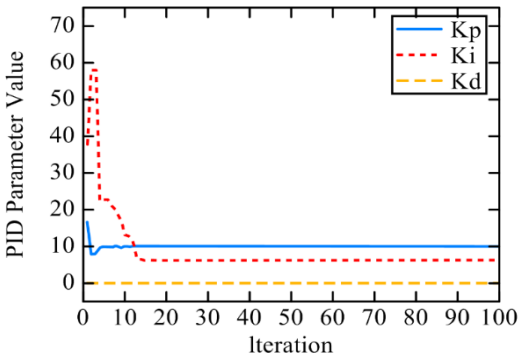

Figure 10: Convergence effect of parameter adjustment of ABC algorithm

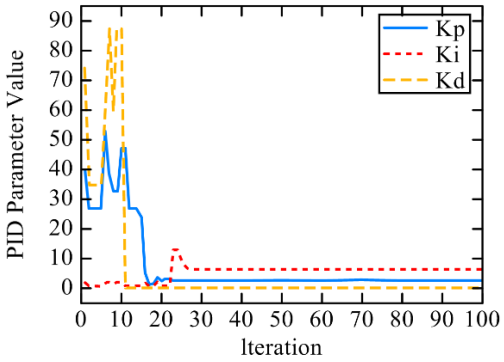

Figure 11: Convergence effect of parameter adjustment of GA algorithm

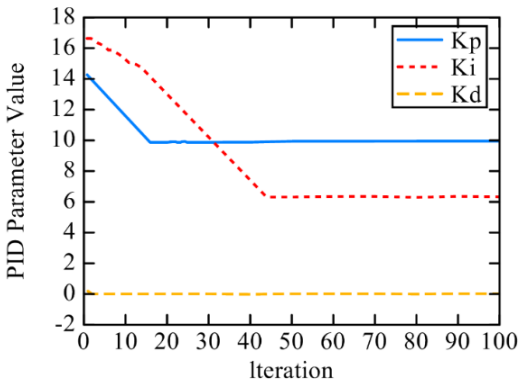

Figure 12: Convergence effect of parameter adjustment of FLA algorithm

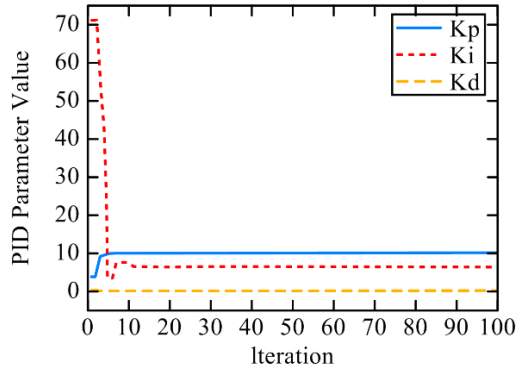

Figure 13: Convergence effect of parameter adjustment of PSO-ABC algorithm

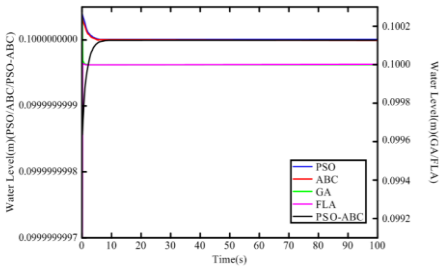

Figure 14: Ballast tank water level height change under five algorithms.

4.3 PID Parameter Adjustment Effect

In order to verify the effect of the bio-heuristic algorithm on the rectification of the PID controller parameters of this model, the Simulink visual simulation tool is used here to build the simulation diagram, as shown in Figure 15. According to the previous calculation, the designed PID controller parameters are shown in Table 5, and here the PSO-ABC algorithm is used to rectify the obtained PID parameters. The curves of the system output and error are compared before and after the operation of the PID controller in the case of unit step signal input. This is shown in Figure 16 to Figure 17:

The theoretical calculation of the steady state error of the system under the action of unit step input is as follows:

$$e_{ss}(\infty)=\frac{1}{1+K} \tag{24}$$

Substituting the open-loop gain of this model transfer function $G(s)=\frac{100}{3}\cdot\frac{1}{\frac{10}{3}s+1}$ into Eq. (24) yields the steady state error values as follows:

$$e_{ss}(\infty)=\frac{1}{1+\frac{100}{3}}\approx 0.03$$

According to Figure16 and Table 8, it can be seen that the theoretical calculations agree with the simulation results. Under the condition without PID controller correction, the output of the system with the error stabilizes in a long enough time, and the error exists all the time and cannot reach the expected value. The system with the addition of the PID correction link can quickly realize the correction of the system deviation, so that the error converges to 0 rapidly, and the fast, accurate and stable operation of the diving robot in underwater levitation is verified in the theoretical simulation.

Table 7. PID Controller Parameter Setting

PID controller parameters	Values
Proportional	9.9371
Integral	6.3231
Derivative	0

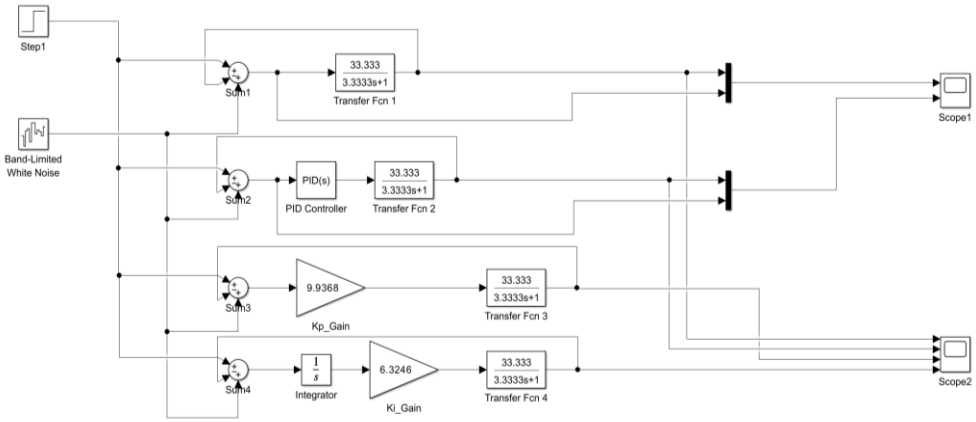

Figure 15: Control system simulation diagram

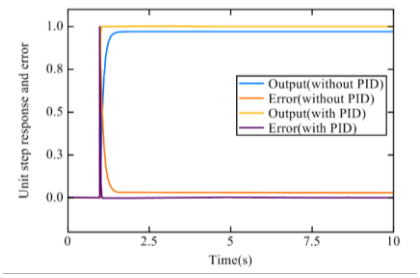

Figure 16: Plot of output as a function of error before and after calibration of the control system

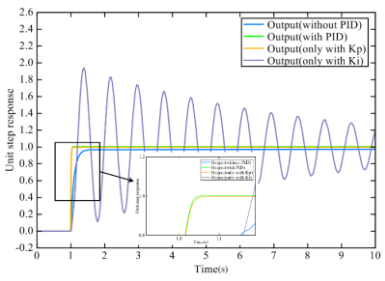

Figure 17: Comparison of calibration output results of the system under different controller conditions

According to Figure 17, it can be seen that when the system is calibrated with only the proportional controller, the results are very close to those with the PID controller. However, zooming in on the details shows that at the beginning of the response, the results of the proportional-only condition are slightly worse than those of the PID condition, and the PID condition eventually converges to 0.9999, while the proportional-only condition only converges to 0.9968. For systems that do not require a high degree of precision, this error can be allowed to exist. However, for higher order, more complex or more sophisticated diving robot models, the proportional controller correction alone will not be able to meet the demand for levitation control. At this point adding an integral controller can have the effect of eliminating the residual difference, making the calibration value closer to the preset value.

Table 8. Control System calibration observables

Calibration of observables	Value
Output stabilization time (without PID)	1.75
Output quantity (without PID)	0.97
Error quantity (without PID)	0.03
Output stabilisation time	1.07
Output quantity	1.00
Error quantity	0

4.4 The Effectiveness of Second-order and Third-order Systems

In order to further demonstrate the effectiveness of parameter tuning for the improved PSO-ABC algorithm PID controller, the transfer function models of the second-order and third-order systems are calibrated separately. The initialization parameter settings of the algorithm are consistent with Table 5, and the system transfer function models are shown in Table 9.

Table 9. System Transfer Function Table

System Type	Transfer function
Second-order system	$G_1(s)=\frac{0.5}{0.01s^2+0.14s+1}$
Third-order system	$G_2(s)=\frac{0.5}{0.1s^3+0.5s^2+s+1}$

In both systems, the algorithms rapidly achieved iterative convergence, with a process similar to that of the first-order system. The specific values of the proportional, integral, and derivative coefficients are shown in Table 10:

Table 10. PID Parameter Tables for Second-Order and Third-Order Systems

PID controller parameters	Second-order system	Third-order system
Proportional	1.9903	1.9606
Integral	0	0
Derivative	0.34435	1.9415

As shown in Figure 18, the simulation schematic for second-order and third-order systems was constructed, including step response diagrams for systems without any correction stages, systems with only proportional control, systems with only derivative control, and systems with PID controllers after correction. Since this algorithm optimizes PID parameter tuning to achieve zero integral term parameters, systems containing only integral stages are no longer tested.

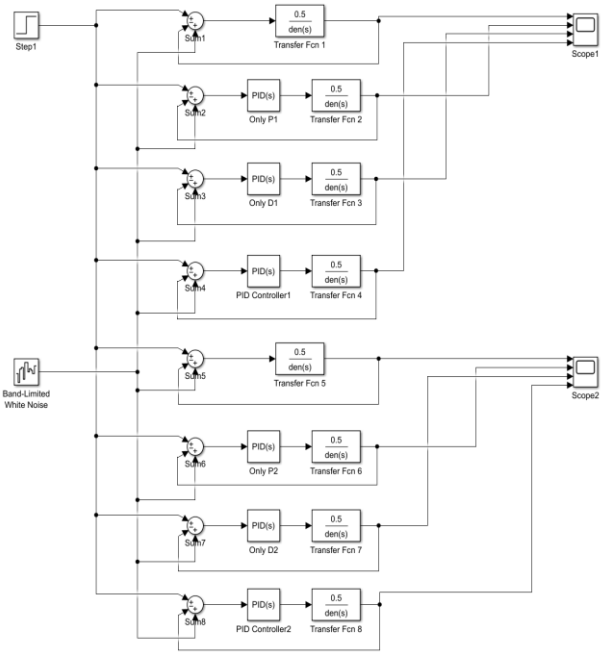

Figure 18: Simulink Simulation Schematic

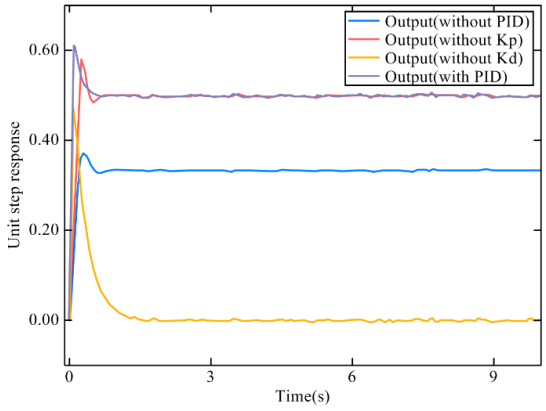

Figure 19: Step Response Diagrams Before and After Second-Order System Correction

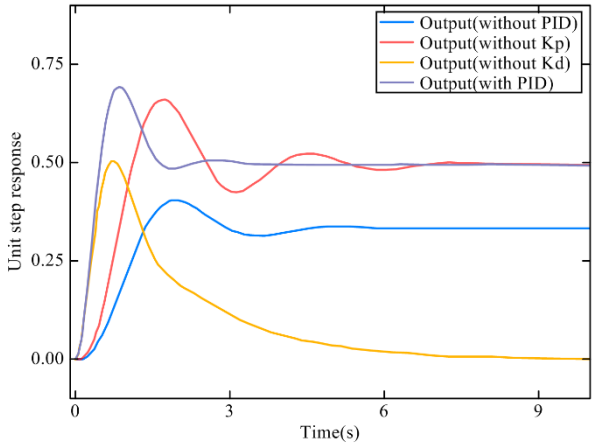

Figure 20: Step Response Diagrams Before and After Third-Order System Correction

In general, an open-loop transfer function with numerator order m and denominator order n can be expressed as:

$$G(s)H(s)=\frac{K\prod_{i=1}^{m}(\tau_i s+1)}{s^{v}\prod_{j=1}^{n-v}(T_j s+1)} \tag{25}$$

where K is the open-loop gain, τ_i and T_j are time constants, and v is the number of reps of the poles of the open-loop system at the origin of the s-plane coordinates. The type of the system corresponds to the value of v.

The steady state error of the system is:

$$e_{ss}(\infty)=\lim_{s\to 0}\frac{sR(s)}{1+G(s)} \tag{26}$$

As shown in Figure 19, the stabilized value of the step response of the second-order system without any correction is about 0.338, and the steady state error is 0.662. According to the second-order system transfer function in the above equation, its system type is 0, and the damping ratio ξ = 0.7, which belongs to the underdamped system. At this time, the steady state error of the calculated system is:

$$e_{ss}(\infty)=\lim_{s\to 0}\frac{s}{1+\frac{0.5}{0.01s^2+0.14s+1}}\cdot\frac{1}{s}=\lim_{s\to 0}\frac{0.01s^2+0.14s+1}{0.01s^2+0.14s+1.5}\approx 0.667$$

As shown in Figure 20, the stabilized value of the step response of the third-order system without any correction is about 0.33, and the steady state error is 0.67. According to the third-order system transfer function in the above equation, its system type is 0. At this time, the steady state error of the calculated system is:

$$e_{ss}(\infty)=\lim_{s\to 0}\frac{s}{1+\frac{0.5}{0.1s^3+0.5s^2+s+1}}\cdot\frac{1}{s}=\lim_{s\to 0}\frac{0.1s^3+0.5s^2+s+1}{0.1s^3+0.5s^2+s+1.5}\approx 0.667$$

The preset calibration value of the PID controllers for both systems is 0.5. When the system is stabilized in the simulation, the step response value is maintained at 0.5, which is in accordance with the design expectations. The input system process in Simulink simulation also includes band-limited white noise signal. The simulation results obtained deviate slightly from the theoretical values.

5. Conclusions

In this paper, the system PID controller parameter tuning is carried out by using bio-heuristic algorithm, which is suitable for computer simulation and large-scale computation. Compared to manual parameter tuning method which consumes labor cost, Ziegler-Nichols relies on physical testing and frequency domain analysis method requires complex process of frequency response testing. In turn, an improved combined particle swarm optimization and artificial bee colony algorithm is designed. Compared with the traditional bio-heuristic algorithm, the algorithm has a significant advantage in the AVG of convergence degree of multiple experiments, STD, and the process of parameter adjustment of the PID controller. And according to the diving robot underwater specific position suspension process to establish a transfer function model, it can be applicated in the PID controller parameter adjustment link, designing corresponding PID controller. Eventually, combining with the theoretical calculation data, building the simulation model verifies the reliability of the algorithm's effect on the water level error correction of the model.

Conflict of Interest

The authors declare that they have no conflicts of interest.

References

[1] Y. Cong, B. Fan, D. Hou, H. Fan, K. Liu, J. Luo. Novel event analysis for human-machine collaborative underwater exploration. Pattern Recognition, Vol. 96, 106967, 2019.

[2] C. Hua, X. Cao, B. Liao, S. Li. Advances on intelligent algorithms for scientific computing: an overview. Frontiers in Neurorobotics, Vol. 17, 1190977, 2023.

[3] H. Du, P. Liu, Q. Cui, X. Ma, H. Wang. PID controller parameter optimized by reformative artificial bee colony algorithm. Journal of Mathematics, Vol. 1, 3826702, 2022.

[4] C. I. Muresan, R. De Keyser. Revisiting Ziegler–Nichols. A fractional order approach. ISA Transactions, Vol. 129, pp. 287-296, 2022.

[5] K. Bingi, R. Ibrahim, M. N. Karsiti, S. M. Hassam, V. R. Harindran. Frequency response based curve

fitting approximation of fractional-order PID controllers. International Journal of Applied Mathematics and Computer Science, Vol. 29, Iss.2, pp. 311-326, 2019.
[6] M. Ahmadnia, A. Hajipour, H. Tavakoli. Robust variable-order fractional PID-LP fuzzy controller for Automatic Voltage Regulator systems. Applied Soft Computing, Vol. 167, 112268, 2024.
[7] K. Saravanakumar, J. S. Isaac. IMO-PSO FO-PID controller-based insulin infusion system for type 1 diabetes patients during post-operation condition. Measurement: Sensors, Vol. 33, 101172, 2024.
[8] R. Baz, K. El Majdoub, F. Giri, O. Ammari. Fine-Tuning Quarter Vehicle Performance: PSO-Optimized Fuzzy PID Controller for In-Wheel BLDC Motor Systems. IFAC-PapersOnLine, Vol. 58, Iss.13, pp. 715-720, 2024.
[9] S. B. Masikana, G. Sharma, S. Sharma, P. N. Bokoro, E. Çelik. Solar PV focused LFC studies utilizing an SFS-optimized PID with fractional derivative (PIDDμ), and incorporating BESS and FESS applications. e-Prime-Advances in Electrical Engineering, Electronics and Energy, Vol. 10, 100787, 2024.
[10] S. O. Amudipe, J. F. Kayode, B. A. Adaramola, O. J. Olatunbosun, S. A. Afolalu. Simulation of transient response of PID controller in an automated electro-pneumatic system using a single-acting cylinder in a clinical ventilator. Heliyon, Vol. 10, Iss.7, 2024.
[11] E. S. Ghith, F. A. A. Tolba. Tuning PID controllers based on hybrid arithmetic optimization algorithm and artificial gorilla troop optimization for micro-robotics systems. IEEE Access, Vol. 11, pp. 27138-27154, 2023.
[12] K. Liu, Y. Fan, J. Chen. A model free adaptive control method based on self-adjusting PID algorithm in pH neutralization process. Chinese Journal of Chemical Engineering, Vol. 76, 2024.
[13] Z. Long, J. Li, H. Yang, W. Chen, G. Zhang, B. Wang, M. Ren. Methods and experiments for automatic control of surface back pressure based on dung beetle optimizer-PID controller. Process Safety and Environmental Protection, Vol. 191, pp. 360-374, 2024.
[14] J. Cheng, B. Zhang, C. Zhang, Y. Zhang, G. Shen. A model-free adaptive predictive path-tracking controller with PID terms for tractors. Biosystems Engineering, Vol. 242, pp. 38-49, 2024.
[15] E. Çelik. Exponential PID controller for effective load frequency regulation of electric power systems. ISA Transactions, Vol. 153, pp. 364-383, 2024.
[16] J. F. Wang, H. Xu, K. Wang, J. Xie, K. S. Yu, G. S. Ye, X. R. Han. Performance analysis and PID control strategy optimization of the electronic expansion valve on the single-tube heat exchange experimental platform. Applied Thermal Engineering, Vol. 250, 123532, 2024.
[17] Y. Wang, Y. Hou, Z. Lai, L. Cao, W. Hong, D. Wu. An adaptive PID controller for path following of autonomous underwater vehicle based on Soft Actor–Critic. Ocean Engineering, Vol. 307, 118171, 2024.
[18] P. Leninpugalhanthi, R. Latha. Adaptive PID controller based direct torque control of fuel cell fed BLDC drive for industryal drives applications. Thermal Science and Engineering Progress, Vol. 55, 102931, 2024.
[19] J. Wang, Q. Zhou, W. Zheng, J. Diao. Trajectory tracking PID passivity-based control of spacecraft formation flying around Sun-Earth L2 point in the port-Hamiltonian framework. Advances in Space Research, Vol. 74, Iss.10, pp. 5086-5099, 2024.
[20] X. Hu, W. Tan, G. Hou. Novel tuning rules for IMC-high-order PID load frequency controller of power systems. Results in Control and Optimization, Vol. 15, 100435, 2024.
[21] S. Chen, P. Xie, J. Liao. Cascade NMPC-PID control strategy of active heave compensation system for ship-mounted offshore crane. Ocean Engineering, Vol. 302, 117648, 2024.
[22] M. Y. Coskun, M. İtik. Intelligent PID control of an industrial electro-hydraulic system. ISA Transactions, Vol. 139, pp. 484-498, 2023.
[23] H. Feng, W. Ma, C. Yin, D. Cao. Trajectory control of electro-hydraulic position servo system using improved PSO-PID controller. Automation in Construction. Advanced Robotic Systems, Vol. 127, 103722, 2021.
[24] K. Vanchinathan, N. Selvaganesan. Adaptive fractional order PID controller tuning for brushless DC motor using artificial bee colony algorithm. Results in Control and Optimization, Vol. 4, 100032, 2021.